www.sciencemag.org/cgi/content/full/322/5899/238/DC1

Supporting Online Material for

Carbon Nanotube Arrays with Strong Shear Binding-On and Easy Normal Lifting-Off

Liangti Qu, Liming Dai,* Morley Stone, Zhenhai Xia, Zhong Lin Wang*

*To whom correspondence should be addressed. E-mail: ldai@udayton.edu (L.D.); zlwang@gatech.edu (Z.L.W.)

Published 10 October 2008, *Science* **322**, 238 (2008)
DOI: 10.1126/science.1159503

This PDF file includes:

Other Supporting Online Material for this manuscript includes the following:
available at www.sciencemag.org/cgi/content/full/322/5899/238/DC1

Supporting Online Materials

Carbon Nanotube Arrays with Strong Shear Binding-On and Easy Normal Lifting-Off

Liangti Qu,[1] Liming Dai,[1,*] Morley Stone,[2] Zhenhai Xia,[3] Zhong Lin Wang [4,*]

* To whom correspondence should be addressed. E-mail: ldai@udayton.edu (L.D.); zlwang@gatech.edu (Z.L.W.)

1. Synthesis of Nanotube Arrays

The vertically-aligned multiwalled carbon nanotube (VA-MWNT) arrays were synthesized by low pressure chemical vapor deposition (CVD) on 4×4 mm^2 SiO_2/Si wafers. A 10-nm thick Al layer was coated on the wafers before the deposition of 3-nm Fe film in order to enhance the attachment of grown nanotubes on the Si substrates. The VA-MWNT arrays can adhere to the growth substrate under a more than 150 N/cm^2 pull force. The catalyst coated substrate was first inserted into the quartz tube furnace (Fig. S1) and remained at 450^oC in air for 10 min, followed by pumping the furnace chamber to a pressure less than 10 mTorr. Thereafter, the growth of the VA-MWNT arrays was achieved by flowing

a mixture gases of 48% Ar, 28% H_2, 24% C_2H_2 at 750^{o}C under 10-100 Torr for 10-20 min. The length of the resultant aligned VA-MWNTs could be adjusted by controlling the deposition time and pressure. During the "base growth" process, the initially formed nanotube segments grew in random directions and formed a "coiled/entangled" nanotube layer. The subsequently continuous growth of straight nanotubes uplifted the randomly entangled nanotube layer, resulting in the formation of the hierarchically structured VA-MWNT arrays with a straight nanotube "forest" covered by the curly entangled top layer.

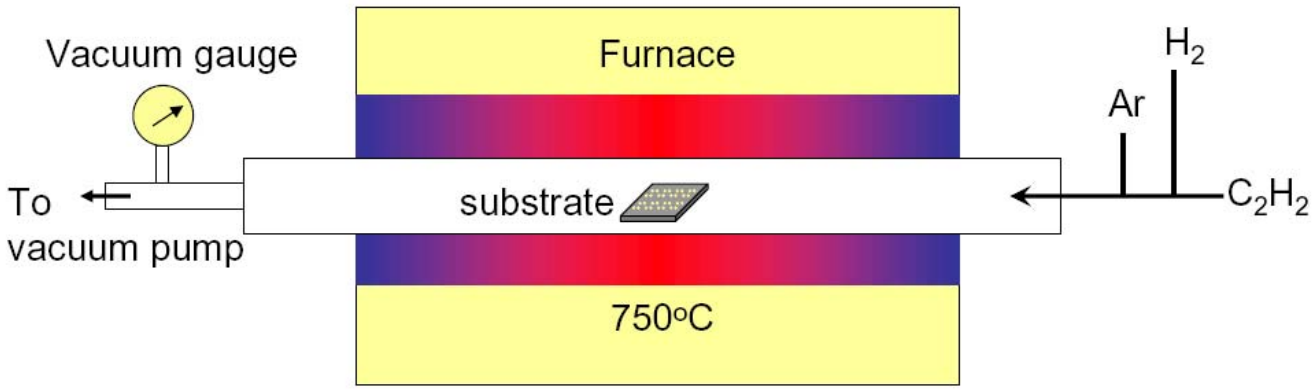

Fig. S1. A schematic diagram of the low pressure CVD system for the growth of VA-MWNT arrays.

We used the reported method (*S1-S3*) for the investigation of the adhesive properties of the aligned MWNT films grown on SiO_2/Si wafers. A preload of about 2 kg was applied to the Si side for pressing the aligned MWNT films against the surface of a glass slide or other substrates. A laboratory balance was used to measure the pull-away force in both the normal and shear directions. In order to eliminate the attachment cycle effect and to avoid the pre-alignment effect for subsequent shear adhesion

measurements, we took adhesion forces from the first measurement on each of the VA-MWNT dry adhesive films, though they can be used for many measurements (typically, we stopped at about 20 times to avoid possible surface contamination caused by multiple measurements, if necessary).

Movie S1*:* Repeated loading of the aligned nanotube dry adhesive attached on a vertically-placed glass plate to hold a heavy object, showing the possibility of repeated operation of sticking-on and lifting-off for mimicking the walking of a gecko. The attaching of the VA-MWNT arrays on the glass surface was repeated twice using the same sample without decrease in the supported weight.

Movie S2*:* Showing the angle-dependence of the adhesion force for a VA-MWNT dry adhesive.

2. Simulation of the Deformation of Nanotube Arrays

This supporting document attempts to demonstrate, by computer simulation, the deformation and failure modes of the hierarchical carbon nanotube arrays as gecko-mimic dry adhesives, observed in the experiment. The deformation was simulated using the model containing 100 VA-MWNT array (10x10) with nonaligned nanotube segments on their top. The details of the simulation are described in Section 2.2, Modeling Methods. The top-end of VA-MWNT array was hold rigidly and pushed downward to a flat surface to apply preloads. After unloading and relaxing, the nanotube array is then pulled upward or laterally. Periodic boundary conditions are applied on the nanotube arrays. The following movies show the deformation of the hierarchical nanotube arrays under loading in normal and shear directions.

2.1. Movies:

A. **Normal Detachment** - Nonaligned nanotube segments are peeled from the substrate

Movie S3: Normal pulling

Movie S4: Normal pulling by zooming at the root

B. **Shear Deformation -** Nonaligned nanotube segments are stretched along substrate

Movie S5: Shear pulling

2.2. Modeling Methods

The model consists of a number of hexagonally-distributed VA-MWNTs, as schematically shown in Fig. S2 in which each bead or "coarse grain" represents a short nanotube segment (aspect ratio l/d = 1) (*S4*), as shown in Fig. S2a, b. The tube-tube and tube-substrate interactions are realized by van der Waals (vdW) force between these beads. From structural mechanics, the general expression of total potential energy is a sum of energies due to bonded interactions and non-bonded interactions

$$U = \sum \frac{1}{2} k_s (\Delta l)^2 + \sum \frac{1}{2} k_b (\Delta \theta)^2 + \sum \frac{1}{2} k_t [\Delta \phi)^2 + \sum U_V \qquad (1)$$

where Δl, $\Delta\theta$ and $\Delta\phi$ represent the bond stretching increment, the bond angle change, and the angle change of bond twisting, respectively. The first three terms on the right-hand side of Eq.1 are energies for axial tension, bending and torsion, respectively, and the last term is the energy of non-bonded interaction. k_s, k_b and k_t in Eq. 1 are the stretching, bending and torsion constants, respectively. From a structural mechanics viewpoint, the deformation of a space frame results in the change of strain energy.

Since the nanotubes are round cross-section, only three stiffness parameters, i.e., tensile stiffness (EA), bending stiffness (EI) and torsional rigidity (GJ), need to be determined for deformation analysis. A direct relationship between the structural mechanics parameters and the molecular mechanics force field constants (*S5*) can be established as: $k_s = EA/L;\ k_b = EI/L;$ and $k_t = GJ/L$, where l is the length of the nanotube segment.

The non-bonded energy U_v in Eq. 1 includes tube-tube and tube-substrate interactions. The tube-tube interaction energy is determined by the integrating Lennard-Jones potential (*S6*) and can be approximated as:

$$U(r) = \pi^2 \rho_s \rho_c R\left[\frac{A}{1620r^7} + \frac{B}{6r}\right] \tag{2}$$

where A and B are Lennard-Jones parameters, ρ_c and ρ_s are the density of VA-MWNTs and substrate, respectively, R is the radius of nanotubes and r is the distance between substrate and bead. The tube-tube interaction potential takes the same form as Eq.2 according to analytical form. In the case of fiber-fiber interaction, ρ_s is replaced by ρ_c. The friction between the nanotube and substrate follow the Amontons friction law: $F_f = F_0 + \mu F_n$, where F_n is the normal force applied on the nanotube and μ is the friction coefficient. The friction force relationship has been confirmed by a fully atomistic simulation.

The deformation was simulated using the model containing 100 nanotubes (10x10). The nonaligned nanotube segments were generated on the top of VA-MWNT arrays (Fig. S2c). The top-end of nanotube array is hold rigidly and pushed downward to a flat surface to apply preloads. After unloading and relaxing, the VA-MWNT array is then pulled upward or laterally. Periodic boundary conditions (in the directions perpendicular to VA-MWNTs) are applied on the nanotube arrays.

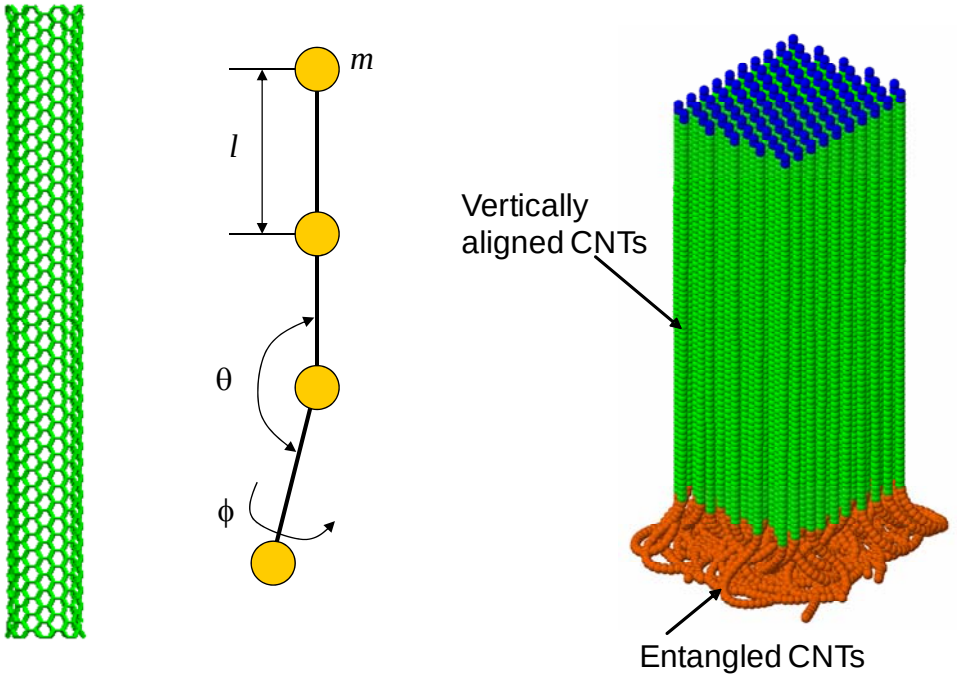

(a) (b) (c)

Fig. S2. (a) Single carbon nanotube, (b) bead model representing nanotube segments and (c) large-scale model consisting nonaligned nanotube segments and VA-MWNT array

3. Adhesion of VA-MWNT Arrays on Various Surfaces

VA-MWNT arrays were found to show strong adhesion to a wide range of surfaces with different flexibilities and surface characteristics, including ground glass, polytetrafluoroethylene (PTFE) film (Swagelok), rough sandpaper (1500-b, GatorGrit, Finland, roughness: ~1.2 μm), and poly(ethylene terephthalate) (PET) sheet (3M), even without cleaning (Figs. S3-6).

Although the shear adhesion forces against rough (*e.g.* sandpaper, ground glass) and/or fluorinated (*e.g.* PTFE) surfaces reduced by a factor of 2-5 with respect to that of a smooth glass plate, the normal adhesion force remained almost unchanged (close to 10 N/cm^2) for all of the substrates studied. Besides,

both the shear and normal adhesion forces measured on the PET sheet reproduce well the corresponding results shown by Figure 1D for the smooth glass plate. As the surface of the commercially available PTFE film is also rough (See, Fig. S5(a)), the observed reduction in the shear adhesion on rough substrates is not inconsistent with Figure 1E, showing a reduced pull-off force with increasing the pull-away angle.

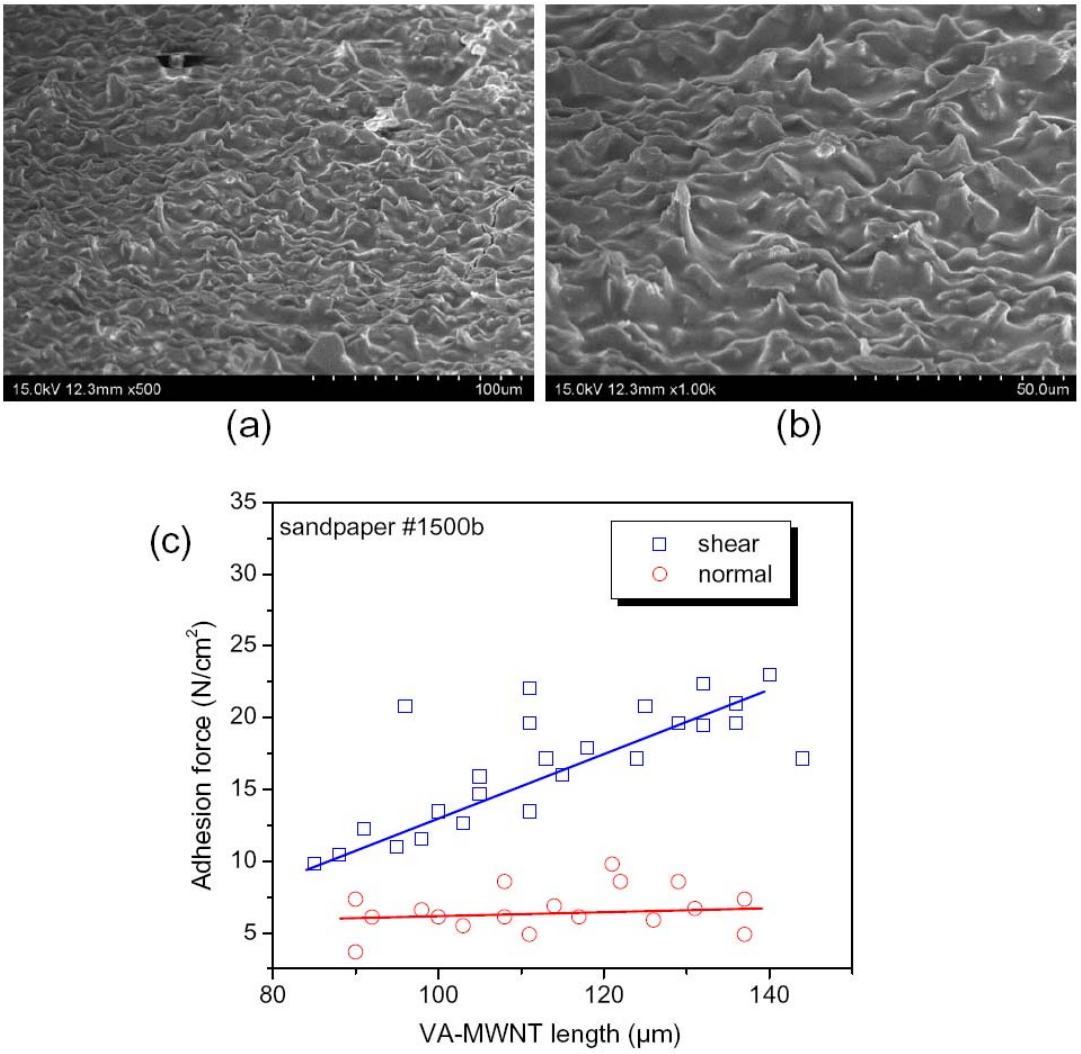

Fig. S3. (a, b) Scanning electron microscopy (SEM) images of commercial sandpaper surface (1500b, Finland), showing quite rough surface with about 5-10 μm high grains, and (c) the corresponding adhesion force of VA-MWNT arrays with different length on the sandpaper.

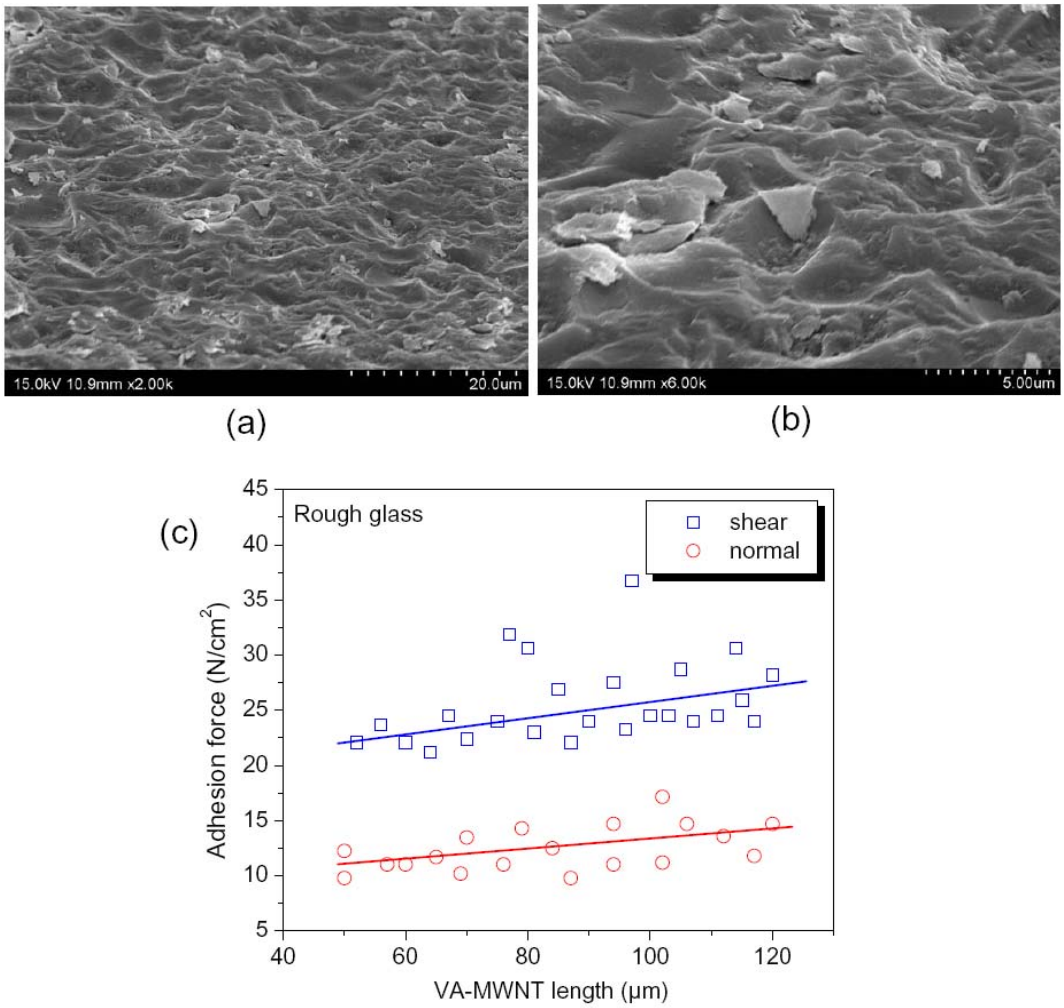

Fig. S4. (a, b) SEM images of ground glass surface, showing several micron deep pits with some dirts, and (c) the corresponding adhesion force of VA-MWNTs with different length on this surface.

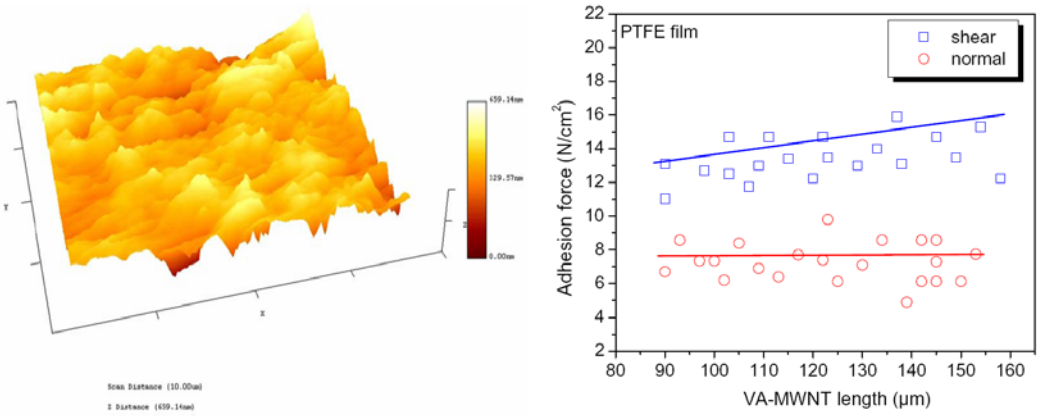

(a) (b)

Fig. S5. (a) AFM image of PTFE (Teflon) surface (roughness: ~80 nm) and (b) the corresponding adhesion force of VA-MWNT arrays with different lengths.

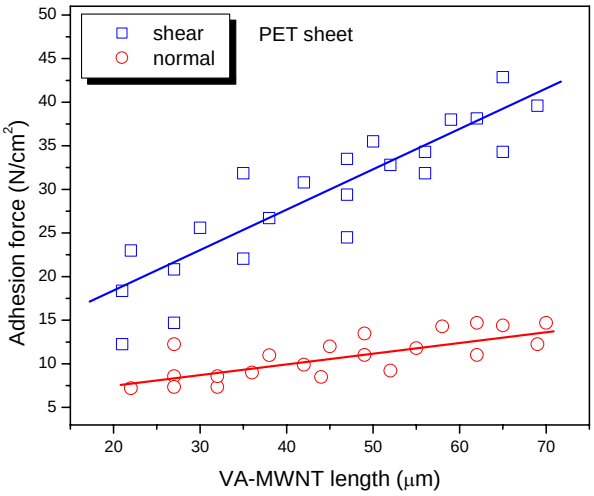

Fig. S6. Adhesion forces of VA-MWNTs with different length on smooth PET sheet.

4. Surface Polarity (Hydrophobic or Hydrophilic) Effect on Adhesion Force

We have measured the adhesion on smooth glass plates before and after a plasma coating that changes the surface polarity/hydrophilicity. The acetic acid (CH_3COOH)-plasma treatment led to a

highly hydrophilic COOH-rich surface while the hexane (C_6H_{14})-plasma treatment produced a hydrophobic hydrocarbon-rich surface. Plasma polymerization was performed on a custom-built plasma apparatus with the monomer pressure for acetic acid and hexane to be 0.1 and 0.55 Torr, respectively, at 200 kHz, 20 W for ~1 min.

As seen in Fig. S7, the adhesion forces increased slightly with increasing the surface hydrophilicity. This indicates that hydrogen bonding may contribute to the measured adhesion force. However, the electrostatic charging based adhesion seems to be negligible (Fig. S8). These results indicate the vdW forces play a dominate role in adhesion between the carbon nanotubes and substrate surface.

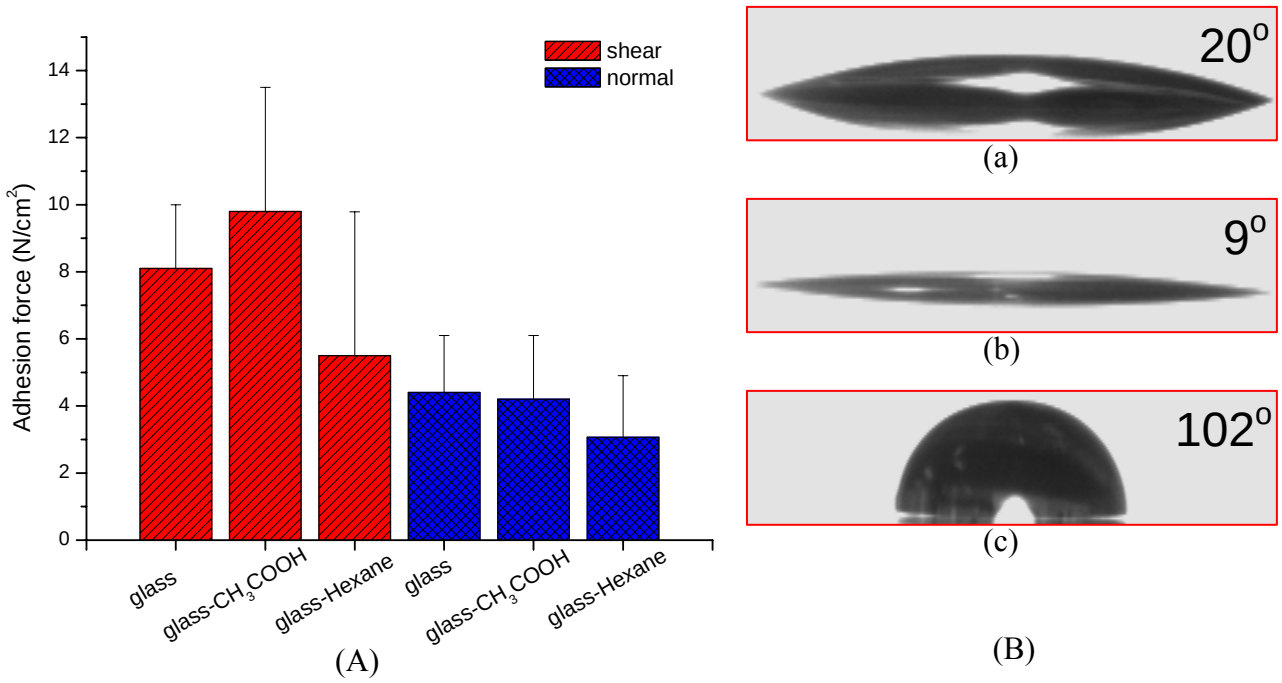

Fig. S7. (A) Comparison of adhesion forces of VA-MWNTs (95±4 μm long) on CH_3COOH- and C_6H_{14}–plasma-treated glass surface (preload: 400g). (B) Water/air contact angles for the pristine glass surface (a); the CH_3COOH-plasma treated glass surface that is rich of COOH groups showing a high hydrophilicity (b); and the C_6H_{14}–plasma-treated glass surface that is rich of hydrocarbon moieties showing a high hydrophobicity (c).

5. Surface Electrostatic Effect on Adhesion Force

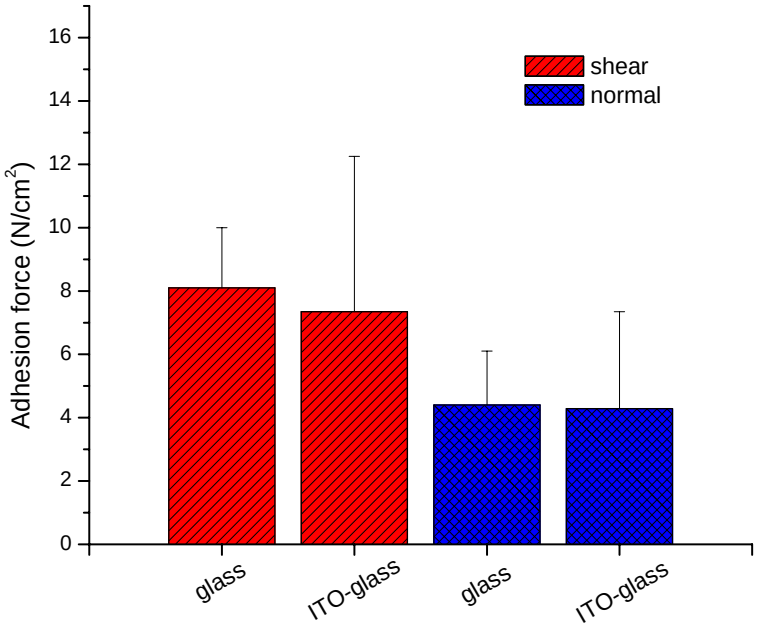

Fig. S8. Comparison of adhesion forces of VA-MWNTs (95±4 μm long) on glass and ITO glass (connected with ground to eliminate the possible electrostatic charging) surface (preload: 400g). No obvious effect of possible electrostatic charging between carbon nanotubes and surfaces on the adhesion force was observed.

6. Durability of VA-MWNT Array Dry Adhesive

Results from the time-dependent adhesion measurements are shown in Figs. S9-11. As seen in Fig. S9, the VA-MWNT dry adhesive (60-μm long) under a shear loading of 40 N/cm^2 or a normal pull-away force of 12 N/cm^2 for more than 24 hours remained on the glass substrate stably without any cohesive breakage. In contrast, the commercial copper adhesive (3M) tapes under the same applied

forces fatigued easily and were peeled away from the substrate within 1 h. Therefore, the enhanced shear adhesion for the nanotube dry adhesive relies on the alignment of the curly entangled nanotube segments, rather than the plastic deformation as for polymer fibers. This point was further checked by devising a setup shown in Figure S10a, where the normal adhesion (F_N) was measured whilst the nanotube adhesive was pre-sheared by a force Fs. Figure S10b shows that the normal adhesion force slightly increased with the side contact due to the nanotube alignment, as predicated by an earlier theoretical study (*S7*). Similar alignment effect was also observed in the shear direction. As shown in Fig. S11, the shear adhesion force increased significantly after the stepwise shear loading for pre-alignment of the nanotube segments.

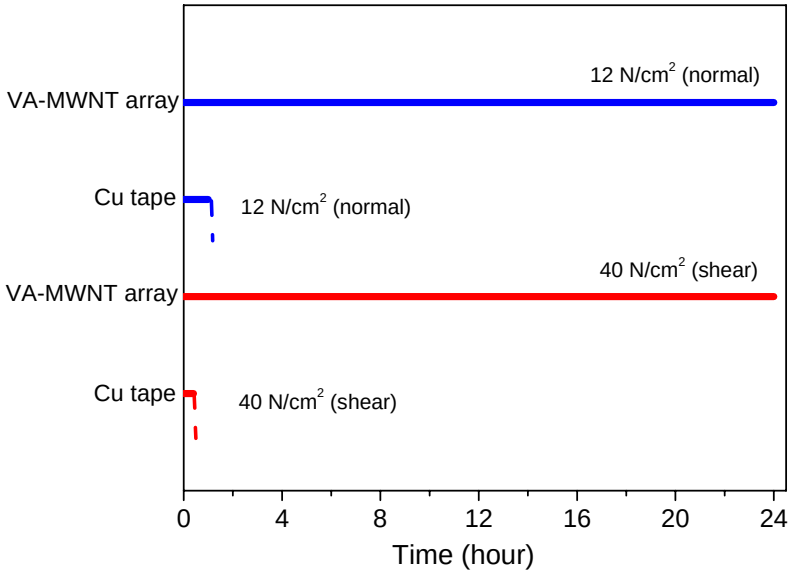

Fig. S9. Durability comparison of commercial copper adhesive tape (3M) and VA-MWNT array (60 μm long) at 40 N/cm^2 shear loading and 12 N/cm^2 normal loading, respectively. The shear and normal forces supported by the nanotube arrays are very stable and last for a long period (*e.g.* 24h) without any cohesive breakage. The commercial copper tapes under the same conditions fatigue easily and were peeled away from the substrate (glass plate) within 1 h.

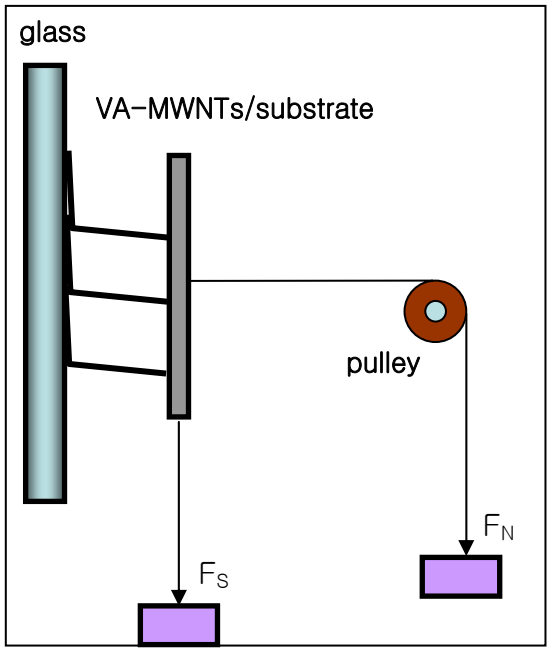

(a)

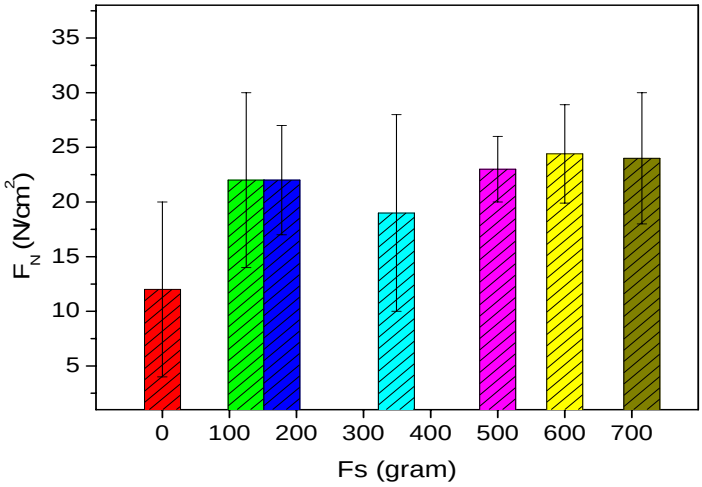

(b)

Fig. S10. (a) A setup for the normal adhesion force measurement under shear pull, and (b) the corresponding normal adhesion force with different loadings in the shear direction (nanotube length = 90-110 μm).

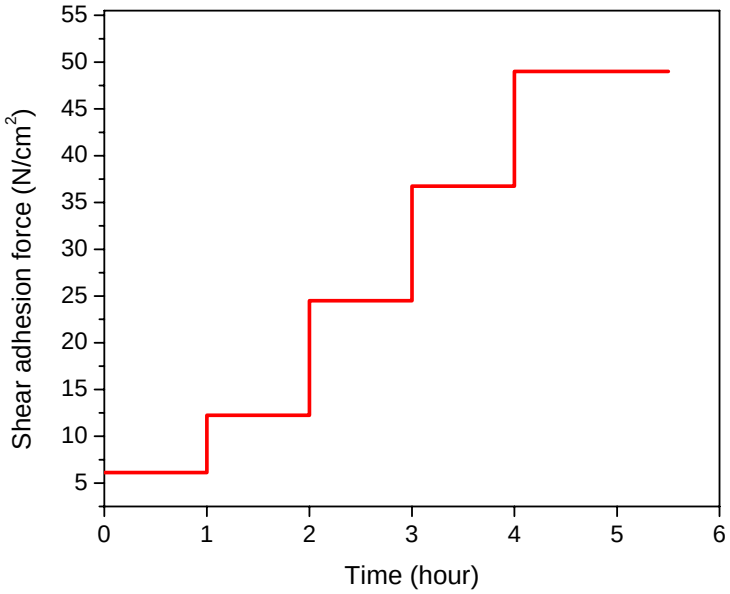

Fig. S11. Different forces (y axis) were applied to a VA-MWNT array (35 μm long) adhered onto a glass plate for 1 hour, showing an enhanced shear adhesion force due to the alignment of nanotubes by the pre-shear treatment. Although the initial sample holds only less than 30 N/cm^2 shear force (See, Fig. 1D) without the pre-shear treatment, the final shear force was measured to be about 50 N/cm^2 after the consecutive shear-pull treatments as shown by the step curves.

7. Effect of Morphology and Surface Chemistry of VA-MWNT arrays on Adhesion Force

We used oxygen plasma etching (*S8, S9*) to remove the nonaligned nanotube segments from a VA-MWNT film to investigate the influence of the nonaligned nanotube surface on the adhesion forces. Fig. S12a shows a typical top-view SEM micrograph for the as-grown VA-MWNT array with some nonaligned nanotube segments on the top surface. After oxygen plasma etching, the nonaligned nanotube segments were largely removed and the perpendicularly-aligned nanotube "trunks" formed

into a bundle-like array due to the polar interaction of the etched nanotube tips (Fig. S12c). The top-view SEM image for the pristine VA-MWNT film after the adhesion force measurements given in Fig. S12b shows the shear-induced alignment. Fig. S12d shows similar features for the oxygen-plasma etched VA-MWNT film after the adhesion force measurements, but with much less horizontally-aligned nanotube segments on the top surface. The removal of the nonaligned nanotube segments by plasma etching largely eliminated the nanotube-length-dependence for both the shear and normal adhesion forces within the experimental error (Fig. S12e). Comparing Fig.S12e with Fig. 1D reveals also a concomitant decrease in both the shear and normal adhesion forces, indicating that the "point" contact is much weaker than the "line" contact (Fig. 2B). However, the plasma-etching-induced "bundle" formation (Fig. S12C), together with surface chemistry changes (Fig. S13), could also weaken the adhesion forces by reducing the number of effective contact points per unit area and/or interaction energy per contact with the glass surface.

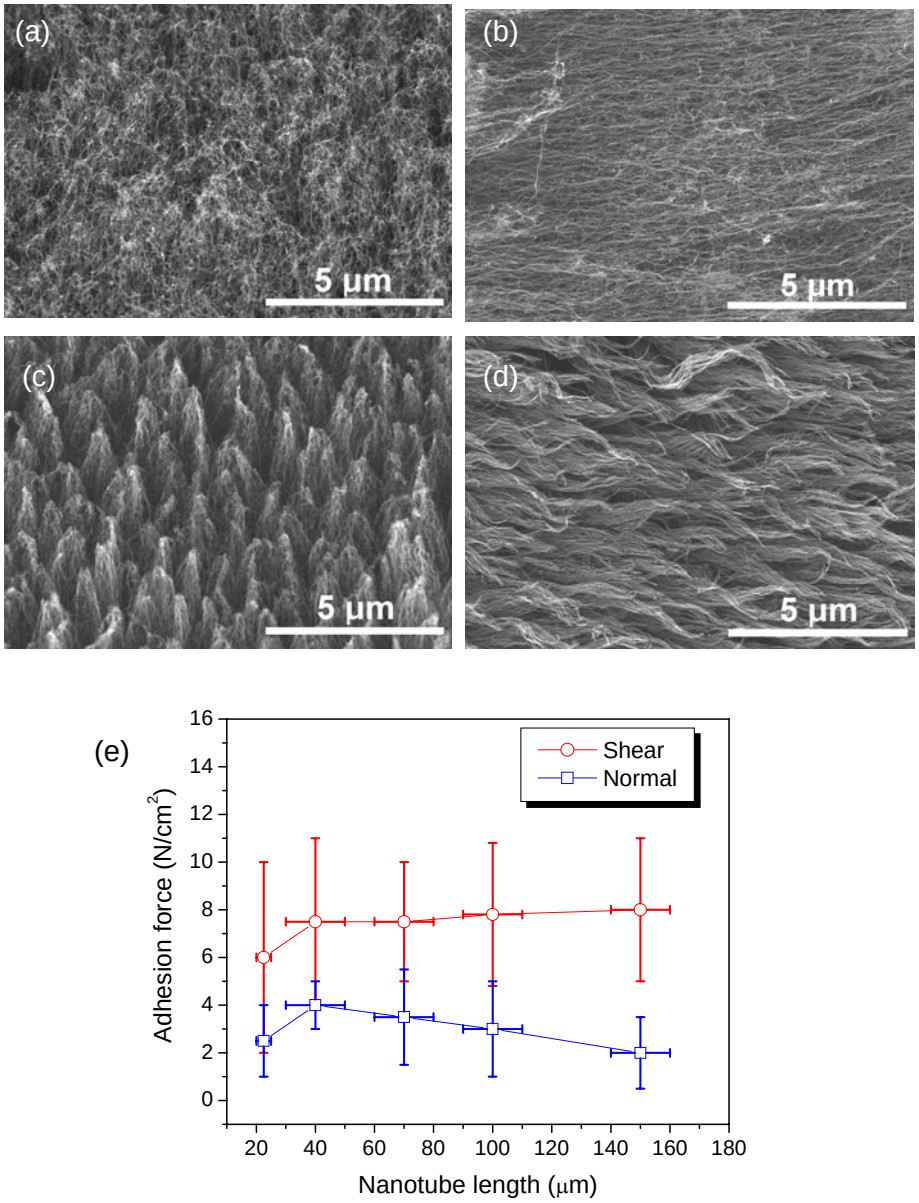

Fig. S12. Effect of the plasma etching on adhesion forces. (a-d) Typical top view of VA-MWNT film before (a, c) and after (b, d) adhesion measurements, (a, b) without and (c, d) with oxygen etching. (e) The dependence of shear and normal adhesions on nanotube length after plasma etching. The vertical and horizontal bars represent the deviations of the force and nanotube length measured for more than 20 samples of the same class, respectively.

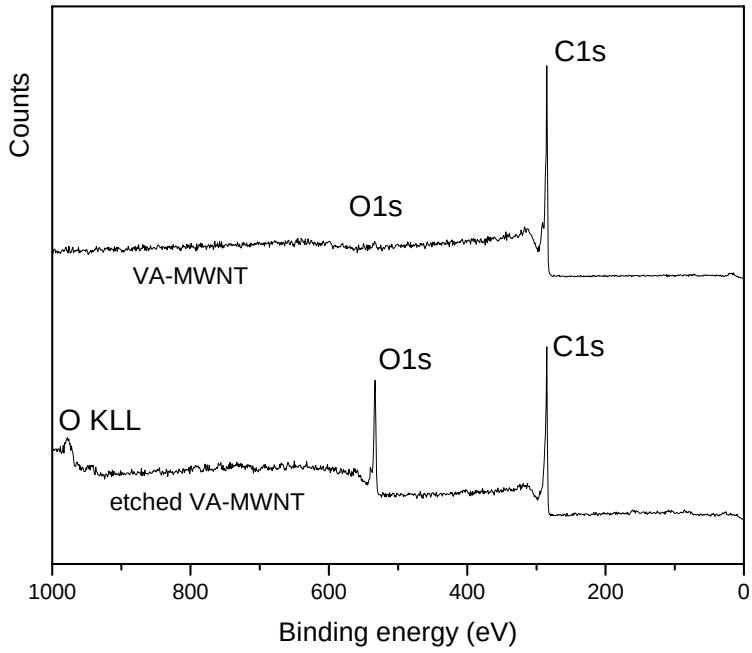

Fig. S13. X-ray photoelectron spectroscopy (XPS) analyses of VA-MWNTs and oxygen plasma etched VA-MWNTs, revealing the oxygen plasma etched VA-MWNTs have strong a peak corresponding to oxygen, and the O/C atomic ratio increases from 0.8% for the pristine VA-MWNTs to 38% for the oxygen plasma etched VA-MWNTs.

To study the influence of nonaligned nanotube segments on the adhesion forces in a more precise way, we eliminated nonaligned nanotube segments from the top of a VA-MWNT array by turning over the as-synthesized VA-MWNT film with full integrity from the SiO_2/Si wafer onto a polystyrene substrate to keep the nanotube density and surface chemistry largely unchanged. As shown in Fig. S14a, we put the pristine VA-MWNT arrays top-side-down into a thin film (~200 μm thick) of melt polystyrene at approximate 245^{o}C. The polystyrene used here has a Mw = 350,000, Tg (glass transition temperature) ≈105 ^{o}C, Tm (melting point) ≈180 ^{o}C, and Tc (decomposition temperature) ≈ 350 ^{o}C. After cooling down to the room temperature, the VA-MWNT arrays are firmly bonded with polymer film.

Upon removal of the VA-MWNTs together with the polymer-support and turning it up side down, the entangled nanotube segments initially on the top of the VA-MWNT array are embedded into the polymer matrices and well-aligned nanotube "trunks" stand upright (Fig. S12a). Fig. S12 b shows a SEM side view for the inverted VA-MWNT array on polystyrene support. The corresponding enlarged SEM side view in Fig. S12c reveals the absence of entangled nanotube segments from the top of the inverted VA-MWNT array. Furthermore, XPS analyses confirm that the surface chemistry of the VA-MWNT array remains unchanged after the inverting process (Fig. S15).

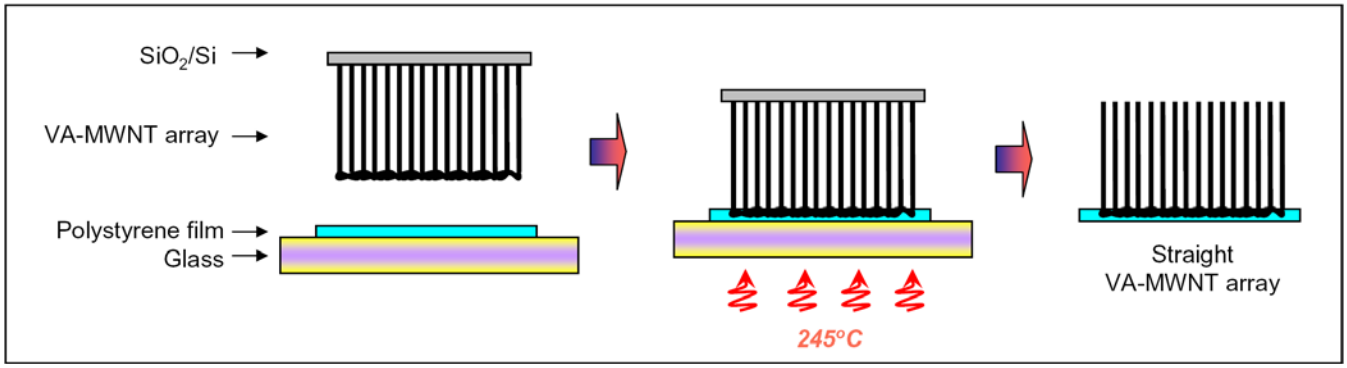

(a)

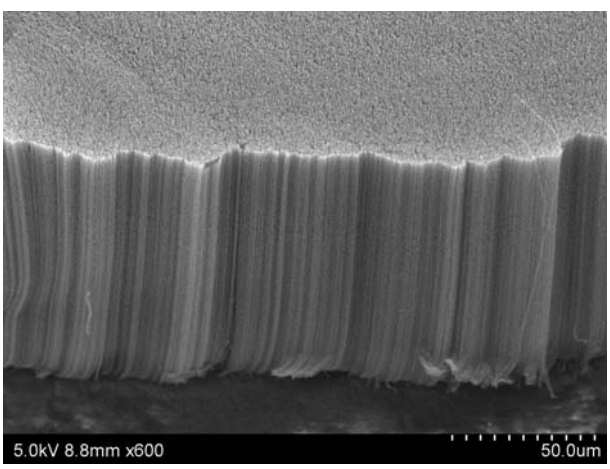

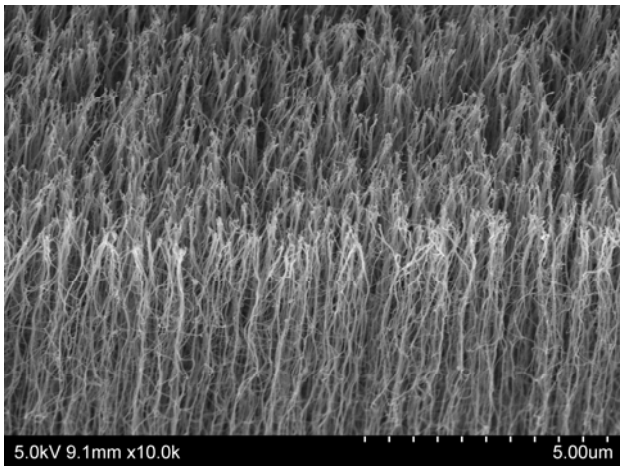

(b) (c)

Fig. S14. (a) Schematic representation of the transfer process to invert the VA-MWNT array onto a polystyrene thin film, (b, c) SEM images of the invert VA-MWNT array.

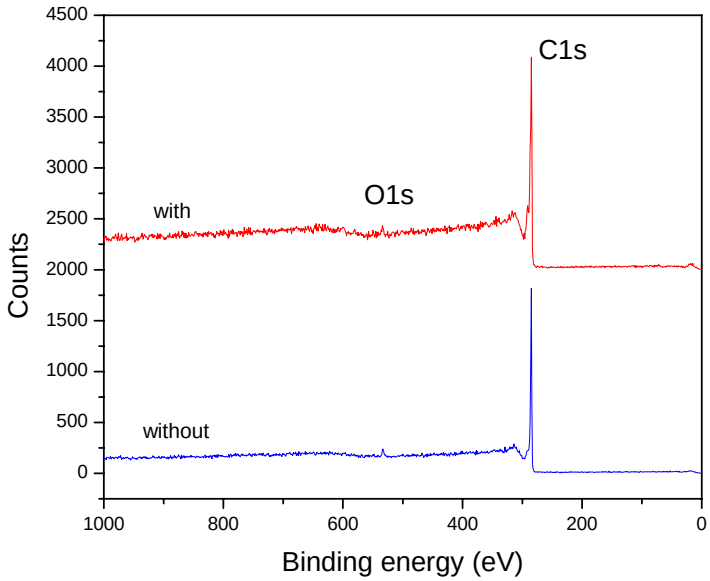

Fig. S15. XPS spectra of VA-MWNTs with and without the top entangled segments by inverting the nanotube array.

8. Effect of Defects and Contaminants of VA-MWNT Arrays on Adhesion Force

To qualitatively demonstrate the effect of defects and contaminants on the adhesion performance of VA-MWNTs, we have deposited amorphous carbon onto the as-synthesized VA-MWNT arrays (Fig. S16a). Amorphous carbon was deposited onto the VA-MWNTs by thermal decomposition of acetylene at 600^{o}C under Ar gas for 5 min. While the transmission electron microscopy (TEM) image shows amorphous carbon coating along the nanotube length (Fig. S16a), Raman spectra reveal an increase in the intensity ratio of D-band/G-band from 0.38 to 0.86 after amorphous carbon deposition (Fig. S16b), indicating that structural defects have been introduced into the amorphous carbon deposited nanotubes. Adhesion force measurements show largely decreases in both the shear and normal adhesion forces for the amorphous carbon coated VA-MWNT arrays (Fig. S16c), indicating that high-quality and clean samples are very important for the observed strong adhesion force.

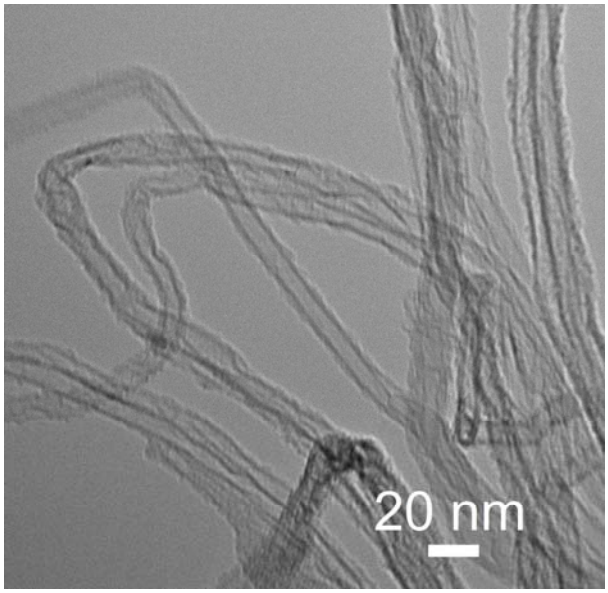

(a)

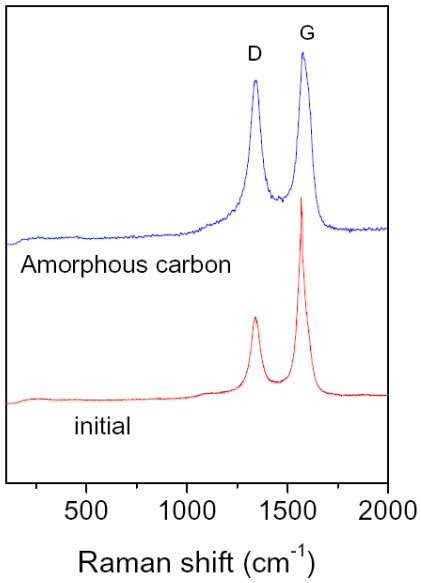

(b)

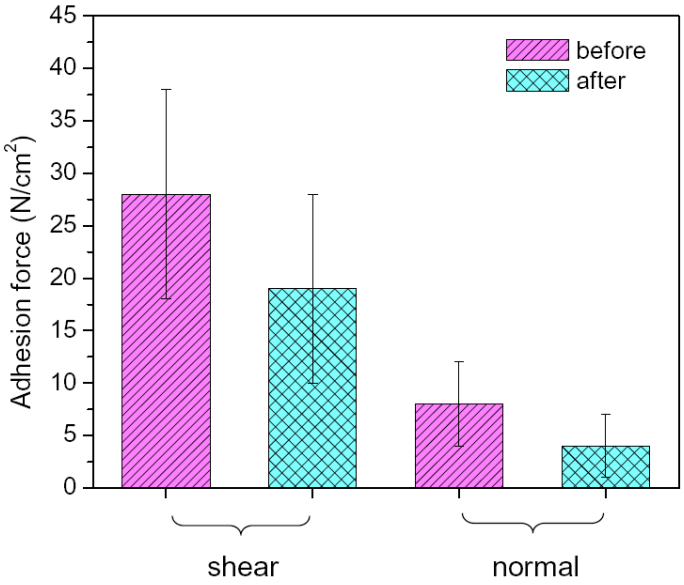

(c)

Fig. S16. (a) TEM image of MWNTs after the amorphous carbon deposition, (b) Raman spectra of the VA-MWNT array before and after the amorphous carbon deposition (514nm laser), and (c) adhesion forces measured for the VA-MWNT array (~ 50 μm long) before and after the amorphous carbon deposition.

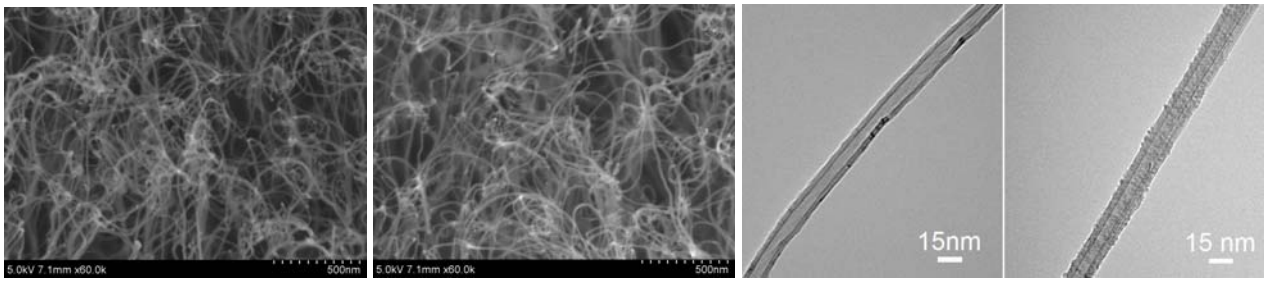

(a) (b) (c) (d)

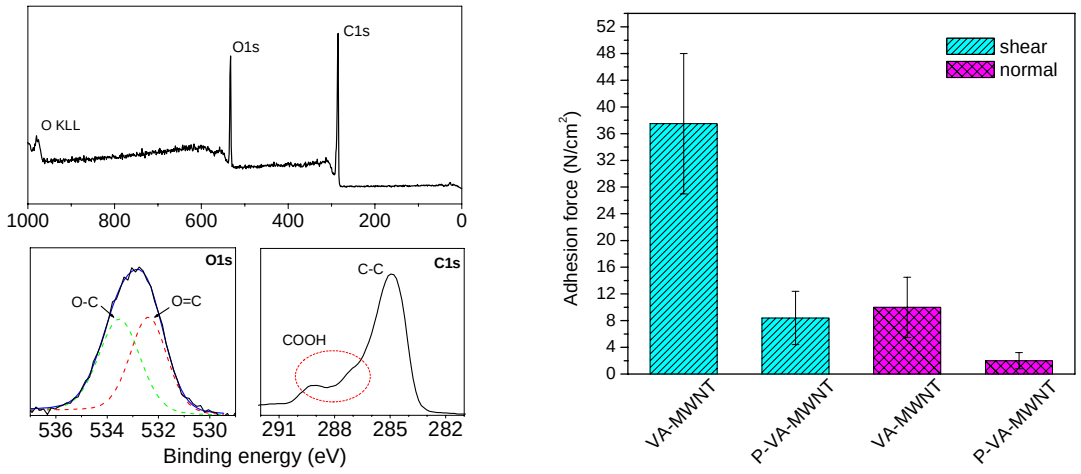

(e) (f)

Fig. S17. (a, b) Top-view SEM images of the VA-MWNT array before (a) and after (b) plasma polymerization of acetic acid; (c, d) TEM images of individual VA-MWNT before (c) and after (d) plasma polymerization of acetic acid; (e) XPS of VA-MWNTs after plasma polymerization of acetic acid; (f) adhesion performance of VA-MWNT arrays (~65-75 μm long) before and after plasma polymerization of acetic acid (P-VA-MWNT).

To further change the nanotube surface chemistry without changing the VA-MWNT structure (*e.g.* packing density and morphology), we have coated the VA-MWNT arrays with plasma polymers by plasma polymerization of acetic acid (*S10*). The top surface of VA-MWNT arrays shows similar features before and after plasma polymerization (Fig. S17, a, b), indicating the plasma polymerization

did not change the geometry of VA-MWNTs. However, TEM images reveal that a layer of thin (less than 1 nm) plasma polymer coating has formed along the nanotube length after plasma polymerization (Fig. S17c, d). The plasma coating was also confirmed by XPS measurements, which revealed the presence of oxygen-containing groups with the O-C/O=C ratio being close to 1 (Fig. S17e). Like the amorphous carbon coating (Fig. S16c), the plasma polymer coating dramatically reduced both the shear and normal adhesion force without changing the ratio of shear to normal strength (Fig. S17f).

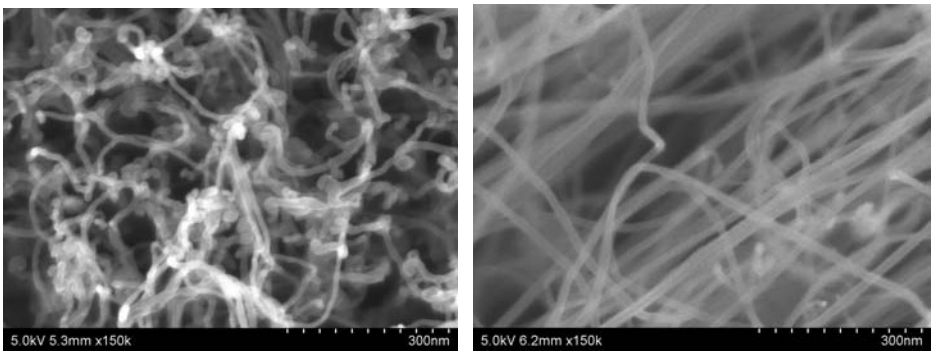

(a) (b)

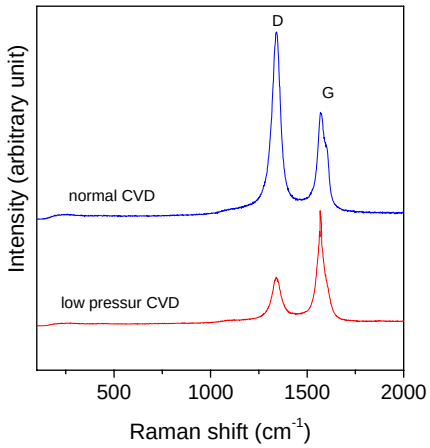

(c)

Fig. S18. High magnification top-view SEM images (a, b) and Raman spectra (c) of VA-MWNTs prepared by atmospheric (conventional) CVD (a) and low pressure CVD (b), indicating high yield defects associated with the former.

References

S1. Y. Zhao, T. Tong, L. Delzeit, A. Kashani, M. Meyyappan, A. Majumdar, *J. Vac. Sci. Technol. B* **24,** 331 (2006).

S2. L. T. Qu, L. M. Dai, *Adv. Mater.* **19,** 3844 (2007).

S3. L. Ge, S. Sethi, L. Ci, P. M. Ajayan, A. Dhinojwala, *Proc. Natl. Acad. Sci. U.S.A.* **104,** 10792 (2007).

S4. Z. H. Xia, J. Y. Liang, "Biomimetic Nanocontact and Adhesion of Carbon Nanotubes for Dry Adhesives", Proceedings of 2006 MRS Meeting, Boston, (2006), online http://www.mrs.org/s_mrs/sec_subscribe.asp?CID=8863&DID=198119&action=detail.

S5. C.Y. Li, T.W. Chou, *Mechanics of Materials* **36**, 1047 (2004).

S6. D. Leckband, J. Israelachvili, *Quarterly Reviews of Biophysics* **34**, 105 (2001).

S7. C.S. Majidi, R.E. Groff, R.S. Fearing, *J. Appl. Phys.* **98**, 103521 (2005).

S8. X. K. Lu, H. Huang, N. Nemchuk, R. S. Ruoff, *Appl. Phys. Lett.* **75,** 193 (1999).

S9. S. M. Huang, L. Dai, *J. Phys. Chem.* **106,** 3543 (2002).

S10. M. Notara, et al. *J Mater Sci: Mater. Med.* **18**, 329 (2007).